Published in final edited form as:
Neuron. 2014 August 20; 83(4): 919–933. doi:10.1016/j.neuron.2014.07.026.

Fear and safety engage competing patterns of theta-gamma coupling in the basolateral amygdala

Joseph M. Stujenske[1], **Ekaterina Likhtik**[2], **Mihir A.Topiwala**[2,3], and **Joshua A. Gordon**[2,3]

[1]Graduate Program in Neurobiology and Behavior, College of Physicians and Surgeons, Columbia University, New York, NY 10032 USA

[2]Department of Psychiatry, College of Physicians and Surgeons, Columbia University, New York, NY 10032 USA

[3]Division of Integrative Neuroscience, New York State Psychiatric Institute, New York, NY 10032 USA

Summary

Theta oscillations synchronize the basolateral amygdala (BLA) with the hippocampus (HPC) and medial prefrontal cortex (mPFC) during fear expression. The role of gamma-frequency oscillations in the BLA is less well characterized. We examined gamma- and theta-frequency activity in recordings of neural activity from the BLA-HPC-mPFC circuit during fear conditioning, extinction, and exposure to an open field. In the BLA, slow (40-70 Hz) and fast (70-120 Hz) gamma oscillations were coupled to distinct phases of the theta cycle and reflected synchronous high frequency unit activity. During periods of fear, BLA theta-fast gamma coupling was enhanced, while fast gamma power was suppressed. Periods of relative safety were associated with enhanced BLA fast gamma power, mPFC-to-BLA directionality, and strong coupling of BLA gamma to mPFC theta. These findings suggest that switches between states of fear and safety are mediated by changes in BLA gamma coupling to competitive theta frequency inputs.

Introduction

The initiation and expression of fear states involve synchronized activity in the basolateral amygdala (BLA), medial prefrontal cortex (mPFC), and hippocampus (HPC). Synchronous theta frequency (4-12 Hz) oscillations recorded in the local field potentials (LFPs) of these brain regions reflect synchronized neural firing, believed to facilitate communication between regions in response to aversive stimuli (Adhikari et al., 2010b; Lesting et al., 2011; Paz et al., 2008; Popa et al., 2010; Seidenbecher et al., 2003). Further, dynamic shifts in BLA-mPFC-HPC theta synchrony have functional relevance to successful consolidation of conditioned fear during paradoxical sleep (Popa et al., 2010), extinction of conditioned fear (Lesting et al., 2013), and discrimination between aversive and safe cues (Likhtik et al.,

2014). Thus, synchronous activity in this circuit is highly relevant to the signaling of both fear and safety.

Another oscillation that has been ubiquitously observed across cortical and subcortical structures is in the faster, gamma frequency range (30-120 Hz,Buzsáki and Wang, 2012). Due to their fast temporal dynamics, gamma oscillations provide the ideal mechanism to coordinate precise neural coding within and across structures (Buzsáki and Wang, 2012; Lisman and Jensen, 2013). Indeed, gamma oscillations are prominent in circuits underlying sensory processing and cognitive functions (Fries, 2009) and their perturbation has been noted in schizophrenia (Cho et al., 2006), underscoring their importance for neural circuit function. In HPC, discrete bands of gamma oscillations are nested within the lower frequency theta oscillation (Belluscio et al., 2012). Importantly, distinct gamma frequency bands have been implicated in differentially synchronizing CA1 with CA3 or medial entorhinal cortex (Colgin et al., 2009). These findings support the notion that theta-coupled gamma oscillations may be fundamental to synchronizing activity within and between regions.

Recently, there has been some evidence for the functional importance of gamma oscillations in the amygdala as well. A 40 Hz gamma oscillation couples the activity of the amygdala, rhinal cortices, and striatum during an appetitive learning task (Bauer et al., 2007; Popescu et al., 2009). Moreover, fear-related gamma oscillations in the BLA have been recently demonstrated (Courtin et al., 2013). Thus, as in HPC, gamma frequency oscillations may be essential for information transfer to and from amygdala nuclei. Given the role of theta frequency oscillations in generating and maintaining fear states, and the strong relationship between theta and gamma in HPC (Belluscio et al., 2012), we hypothesized that BLA theta oscillations may coordinate gamma frequency activity in a behaviorally-relevant manner, and, as in the dorsal CA1, gamma oscillations could provide windows for coupling BLA activity to hippocampal and prefrontal inputs.

To test this hypothesis, we recorded simultaneous LFPs in the BLA, mPFC, ventral HPC (vHPC), and dorsal HPC (dHPC), and unit activity in the BLA, during a discriminative fear conditioning paradigm. In the BLA, two distinct bands of gamma-frequency activity were coupled to local theta oscillations, and this theta-gamma modulation was enhanced during fear recall. Surprisingly, though local theta-gamma coupling was weaker during epochs of reduced freezing, power in the fast gamma band (70-120 Hz) was enhanced and reflected an increase in synchronized firing of BLA units. Fast gamma dynamically switched its coupling with behavior, coupling to BLA theta during fear expression (presentation of a CS+), and mPFC theta during safety (presentation of a CS−). We further explored this fast gamma frequency oscillation as a putative safety signal following fear extinction, and in the open field test of innate anxiety. Consistent with a role in safety, the power of this signal was enhanced and associated with a predominant mPFC-to-BLA directionality both following extinction training and in the periphery of the open field. This pattern reflects an enhanced mPFC theta lead over BLA activity, suggesting that synchronization of BLA gamma to mPFC theta is a general mechanism for fear suppression.

Results

To examine gamma frequency activity elicited during fear, mice with chronically implanted stereotrodes in the BLA (Figure S1A-B) as well as microelectrodes in the mPFC, vHPC, and dHPC, were conditioned in a discriminative fear paradigm, as described previously (Likhtik et al., 2014). The mice were exposed to two different auditory stimuli (each presented as one 50 ms pip per second for 30 seconds). One stimulus (CS+) was paired with a mild (0.4 mA) foot shock, while the other (CS−) was explicitly unpaired. On three consecutive training days, animals were presented with five CS+ and five CS− stimuli daily, in a pseudo-random order. On day four, the same stimuli were presented in a new environment without the accompanying shocks, while neural activity was recorded (Figure 1A). Freezing behavior to the CS+ was only weakly attenuated during this fear recall session, with a decrease in mean freezing of 6.4 +/− 4.5% from trial 1 to trial 5 (Figure S1C; $F_{30,1} = 3.74$, $p = .0554$, repeated measures ANOVA); for this reason, data from all five CS+ trials were collectively analyzed.

As previously reported, some mice discriminated appropriately between CS+ and CS− based on their freezing behavior (referred to as discriminators, defined by at least 10% more freezing to the CS+ than the CS−; cutoff determined as in Likhtik et al., 2014), while other mice displayed generalized freezing to both stimuli (generalizers, <10% difference between CS+ and CS− freezing rates). During the CS+, freezing behavior was equivalent between discriminators and generalizers (Figure S1D); thus, we analyzed BLA LFP activity across all animals (n=23) during CS+ presentations on Day 4 to evaluate fear-related activity. In contrast, the explicitly unpaired CS− reflects a potentially aversive stimulus that was successfully associated with safety in discriminators (n=14), allowing us to subsequently evaluate safety-related physiological changes.

Distinct bands of theta-nested gamma in the BLA

Both theta- and gamma-frequency activity was seen in the BLA during the CS+ (Figure 1). We decomposed the signal with wavelets (Supplementary Experimental Procedures) to extract separate frequency components from the ongoing LFP. This analysis revealed two frequencies of gamma oscillations (Figure 1B), which appeared as distinct peaks in the distribution of instantaneous gamma frequency (peaks at 55 and 90 Hz, respectively; Figure S2A). These bands, termed slow (40-70 Hz) and fast gamma (70-120 Hz), could also be separately extracted using bandpass filters (Figure 1B, bottom traces).

In addition to ongoing gamma oscillations, we also observed a prominent sensory-evoked response in the 15-40 Hz range that was largely limited to 0-100 ms following pip onset (Figure S2B). Activity in this pip-evoked band was distinct from slow and fast gamma on the basis of strong power-power correlations within bands but weak correlation between bands (Figure S2C). Likewise, neither slow nor fast gamma was as reliably phase-locked to the pip as the 15-40 Hz pip-evoked band (Figure S2B, D). Overall, these data suggests that there are at least three distinct bands of high frequency activity in the BLA: slow and fast gamma, and pip-evoked 15-40 Hz activity.

In HPC and cortex, lower frequency activity organizes higher frequency oscillations. Given the prominent fear-evoked theta oscillation in the BLA, we investigated whether the

observed BLA gamma oscillations were coupled to theta. We examined both phase-amplitude coupling, where gamma power changes differentially with theta phase, and phase-phase coupling, where a fixed number of gamma cycles occur per theta cycle (Belluscio et al., 2012; Lisman and Buzsáki, 2008). Phase-amplitude coupling was examined using a comodugram to determine the extent by which high frequency (30-150 Hz) power was modulated by low frequency (0-30 Hz) phase (Tort et al., 2009), which we quantified with the mean resultant length (MRL), a measure of circular unimodality (higher MRL indicates that power peaks more reliably at a particular phase). We found that both slow and fast gamma bands were strongly coupled with oscillations in low theta frequencies (4-8 Hz; Figure 1C), consistent with theta evoked by fear recall, which peaks around 6 Hz (Figure 2A; Pape et al., 2005). Additionally, while slow gamma oscillations most often occurred on the trough or early ascending phase of the theta oscillation, fast gamma oscillations occurred closer to the peak or late ascending phase (Figure 1D). Notably, BLA spikes showed a different (though overlapping) pattern of phase-locking compared to gamma (Figure 1D, bottom histograms), suggesting that slow and fast gamma activity could be distinguished from spike-related transients that can contaminate high frequency signals (Ray and Maunsell, 2011). To further explore the nature of theta/gamma relationship, phase-phase coupling was quantified as previously described (Belluscio et al., 2012). Within the BLA, there was significant n:m phase-phase coupling of both slow and fast gamma oscillations to the theta oscillation (Figure S3A-C). This analysis predicts that 9 slow and 15 fast gamma cycles occurred per full theta cycle (Figure S3B), consistent with coupling of a ~55 Hz and ~90 Hz oscillation with a 6 Hz theta oscillation. This analysis strongly supports that both slow and fast gamma represent genuine oscillations, as it would be unlikely for non-oscillatory signals to exhibit phase-phase coupling patterns.

Theta-gamma coupling is enhanced by conditioned fear

Given fear-associated enhancements in amygdala theta power in response to conditioned stimuli (Figure 2A; Likhtik et al., 2014; Popa et al., 2010; Seidenbecher et al., 2003), we asked whether theta-gamma coupling in the BLA was also enhanced during fear. Indeed, we found a pronounced strengthening of theta-gamma coupling during CS+ presentations (Figure 2B) compared to pretone (30 seconds before tone presentation), for both slow and fast gamma oscillations as well as a small band between 15 and 20 Hz ($p<.05/21$, Bonferroni-corrected; Figure 2B). Phase-phase coupling was also significantly stronger during the CS+ than pretone (Figure S3C).

We questioned whether increased theta-gamma coupling was indeed due to enhanced organization of gamma frequency activity by theta or if this was spurious coupling due to independent changes in the theta and gamma range that were each phase-locked to the pip. . To rule out this possibility, we performed two analyses. First, we compared our results to a shift predictor obtained by shifting the gamma power relative to the theta phase by × seconds (where × is an integer value between 1 and 30) so that pip onsets were still aligned. The shift predictor had no strong patterns of theta-gamma coupling (Figure 2B) and thus a significantly weaker strength of theta-gamma phase coupling than the CS+ (Figure 2C; $p<.05/21$, sign-rank). Second, pip-evoked responses (0-300 ms from pip onset) were removed and theta-gamma coupling calculated without these segments; this did not diminish the

strength of coupling for either gamma range (data not shown). Thus, the enhanced theta-gamma coupling during the CS+ is not an artifact of pip structure, but instead suggests a fundamental role for fear-related theta oscillations in organizing high frequency neuronal activity that outlasts the pip.

Theta-fast gamma coupling occurred most strongly when the instantaneous frequency of theta was 6 Hz (Figure 2D), consistent with the peak theta frequency observed during aversive tone presentations (Figure 2A). This 6 Hz coupling peak was absent during pretone. In contrast, slow gamma oscillations were maximally coupled with theta in the 9-10 Hz range, suggesting that slow gamma is relatively insensitive to the fear-evoked 6 Hz oscillation (Figure 2E). There was also significantly greater enhancement in theta-fast gamma coupling from pretone to the CS+ (Figure 2E, right; p=.014, sign-rank), compared to that seen for slow gamma, although both increases were significantly different from pretone (fast gamma, $p=1.57 \times 10^{-5}$; slow gamma, p=.011). For both of these reasons, we focused on the fast gamma oscillation as it relates to fear learning for further analysis.

We asked what property of the fear-evoked theta oscillation accounted for the enhancement in theta-gamma coupling during the CS+. We first tested whether enhanced theta power during the CS+ ($p < 0.001$, sign-rank; Figure S3D) explains the increased coupling. Although there was a direct correlation between theta power and theta phase-gamma power coupling (Figure S3E), it did not exclusively explain the CS+ evoked enhancement in modulation. Considering epochs where theta power fell within equal ranges for both the pretone and CS+ (defined as standard deviations from the pretone mean), theta-fast gamma coupling was enhanced in the CS+ compared to pretone (Figure 2F).

These data suggest that enhancements in both theta power and the strength of theta-gamma coupling are neural signatures of elevated fear. If so, then coupling during the fear-inducing CS+ should be greater than during the explicitly safe CS− in mice that successfully discriminated between the two stimuli. As expected, we observed enhanced theta-gamma coupling during the CS+ compared to the CS– (Figure S3F; p<.01, sign-rank) in discriminators. The CS− was, however, associated with significantly stronger theta-gamma coupling than the pretone (p<.001, sign-rank), falling between pretone and CS+, likely because freezing to the CS−, though diminished, was still above baseline levels (~20%; Figure S1D). Again, these effects were not entirely explained by theta power differences between CS+, CS−, and pretone (Figure S3F). Notably, the increase in theta-gamma coupling from CS− to CS+ was directly correlated with the increase in freezing from CS− to CS+ on an animal by animal basis (Figure S3G; r=.55, p =.007), substantiating enhanced theta-gamma coupling as a novel neural correlate of enhanced fear.

Fast gamma power is reduced in conditioned fear states

We expected that enhanced theta power and theta-gamma coupling during fear should be accompanied by an increase in the strength of gamma oscillations, as has been reported in the auditory cortex (Headley and Weinberger, 2013). Contrary to our expectation, however, BLA fast gamma power was lower during the CS+ than the CS− in discriminators (Figure 3A-B; n=14). In generalizers, there was no significant difference (Figure 3B; n=9). This relationship between relative fear and gamma power also held true when considering

discrimination on a continuous basis: the greater the discrimination between CS+ vs CS−, the greater the difference in fast gamma power (Figure 3C; r=0.48, p<.05). The power change was specific to the fast gamma oscillation, as there was no fear-related difference in power in the slow gamma range (Figure S4A; p>.05, sign-rank). There was also no difference in multi-unit firing rate (Figure S4B; p>.05, sign-rank) or power in higher frequency spectral components (150-800 Hz; p>.05, sign-rank), which followed firing rate changes closely (Figure S5C-D), suggesting that the change in fast gamma power did not reflect spike contamination. These data raise the possibility that activity in the fast gamma range may reflect a novel safety-related signature in the amygdala.

To further test this hypothesis, we evaluated correlations between fast gamma power and defensive behavior within animals on a trial-by-trial basis. Consistent with fast gamma being a safety-signal, freezing rates on individual trials were inversely correlated with fast gamma power, while simultaneously being positively correlated with theta-gamma coupling strength (Figure 3D). Both of these effects were significant across the population (Figure 3E; p<.001 and p<.05, respectively; multiple linear regression, MLR). There was no significant correlation between slow gamma power and trial-by-trial freezing rates, although there was trend towards a positive relationship (Figure S5E; r=.354; p=0.11, MLR). Overall, these data suggest that in the BLA, fear-associated theta simultaneously organizes fast gamma oscillations and decreases their power. This is reversed during safety, when local theta less effectively organizes fast gamma oscillations and fast gamma power is elevated.

Using the motor response of the animal as a measure of fear confounds the internal state (sense of fear or safety) of the animal with its motor response to that state. To disambiguate whether changes in fast gamma power and coupling to theta were associated with either safety or motor response, we performed two additional analyses. First, fast gamma power and theta-gamma coupling were calculated as a function of velocity in the same animals prior to fear conditioning, and second, these measures were calculated during periods of immobility (speed < 5 cm/s), allowing for the comparison of responses to the CS+ and CS− when motor behavior was equivalent. No association was found between fast gamma power and speed (Figure S4G), while for theta-fast gamma coupling, there was an inverted-U relationship with a peak at 6 cm/s, which could not explain our results. Moreover, the effects of stimulus type were present even during immobility epochs alone (Figure S4H-I). Thus, gamma coupling and power appear to be related to behavioral state rather than motor activity.

Fast gamma oscillations reflect BLA neuronal activity

Particularly in a non-laminar structure such as the BLA, the origins of signals recorded in the LFP can be unclear. To confirm that safety-related gamma oscillations reflect local activity, we examined the relationship between BLA gamma and simultaneously recorded multi-unit and single unit activity. All analyses compared unit and LFP activity recorded from nearby but different stereotrodes to eliminate spike contamination of the LFP as a source of error.

We first analyzed recordings of BLA multi-unit activity, which are less subject to volume conduction than the LFP, although such recordings can be dominated by spikes from fast-

spiking interneurons. One third of BLA multi-unit recordings (21/63) had statistically significant phase-locking ($p<.05$, Rayleigh's test) to BLA fast gamma oscillations during the CS+ (Figure 4A-B; $p<.001$ relative to shift predictor, McNemar's test). Spike-spike cross correlations (Supplementary Experimental Procedures) also revealed significant synchrony between simultaneously recorded multi-units during fast gamma oscillations (Figure S5; $p<.001$, sign-rank, n=102 pairs). These findings suggest that gamma oscillations are associated with synchronous neuronal activation in at least a subset of BLA neurons.

Given that discriminators demonstrated enhanced fast gamma power during the CS− compared to the CS+, we anticipated that they would show stronger local gamma-frequency synchrony during the CS−than the CS+. Indeed, we found that in discriminators, a higher percentage of multi-unit recordings were significantly phase-locked to fast gamma oscillations during the CS− than CS+ (Figure 4C; $p<.05$, McNemar's test). Phase-locking to theta or slow gamma was not affected by stimulus type (Figure S4F; $p > .05$), suggesting that this safety-related change is highly specific. We also evaluated the relationship between phase-locking differences and discrimination on a continuous scale (rather than relying on a significance threshold), quantifying phase locking strength, as measured by MRL, for every multi-unit recording. Multi-unit firing of discriminators was more strongly phase locked to fast gamma during the CS−than the CS+ (Figure 4D; $p<.01$, sign-rank). Importantly, for generalizers, the strength of phase-locking to fast gamma did not differ by CS (Figure 4C; $p>.05$, McNemar's test; Figure 4D; $p>.05$, sign-rank). Taken together, these data demonstrate that neural activity in the BLA is synchronized during fast gamma oscillations, and this synchronization is enhanced during stimuli the animal treated as signaling safety.

We next confirmed these findings in recordings of 83 well-isolated single units from the BLA. 18 (21%) of these units exhibited significant phase-locking to the fast gamma oscillation ($p < .05$, Rayleigh test). One such unit is shown in Figure 5A, exhibiting firing phase-locked to the trough of fast gamma oscillations. Likewise, all fast gamma phase-locked single units were coupled close to the trough of the oscillation (Figure 5B). The firing rates of phase-locked units were directly correlated with simultaneously recorded LFP fast gamma power (Figure 5C), suggesting they are involved in generating these oscillations. A signature of this population was that they tended to fire in doublets with interspike intervals < 40 ms (Pape et al., 1998; Figure S6), consistent with models for achieving synchronous gamma frequency activity (Buzsáki and Wang, 2012).

If phase-locked cells are involved in generating the fast gamma oscillations associated with safety, then their activity should be inversely correlated with freezing on short-order time scales. Consistent with this idea, units that were phase locked to fast gamma showed higher firing rates during periods of decreased freezing. An example is shown in Figure 5D, depicting a unit that tended to fire more on trials when the freezing rate of the animal was lower. This relationship was significant for the sample of gamma phase-locked units (Figure 5E; $p<.001$, MLR), but not for non-phase-locked units ($p>.05$). Indeed, when we evenly divided trials into those when the animals froze the most versus those when animals froze the least, we saw a dramatic decrease in firing rate of fast gamma phase-locked units with increased freezing (Figure 5F; $p<.05$, sign-rank). This change was significantly different ($p<.05$, rank-sum) from non-phase-locked units, which were not significantly modulated by

freezing (p>.05, sign-rank). Taken together, these data suggested that strongly phase-locked, doublet-firing units represent putative generators of the fast gamma oscillation.

Gamma synchrony across the cortico-limbic system

Encoding of fear and safety is also believed to engage circuits in the mPFC and HPC, which are highly interconnected and synchronized with the BLA (Lesting et al., 2011). A critical property of gamma oscillations is that they can be tightly synchronized between structures with near zero phase lag, even across long distances (Buzsáki and Wang, 2012). Such tight phase synchrony is suggested to allow for precise temporal coding despite long conduction delays (Buzsáki and Wang, 2012).

Indeed, we observed highly synchronous slow and fast gamma oscillations in all three brain regions (Figure 6). During epochs of strong BLA gamma oscillations (>1.5 SD above mean power), we found that fast gamma oscillations were phase-synchronized across structures, as shown in gamma-triggered traces and coherograms (Figure 6A). Both BLA-mPFC (n=22) and BLA-vHPC (n=11) fast gamma phase-phase differences had a strong peak near 0, which was not found for a shift-predictor (Figure S7A). Similar results were obtained when the BLA was referenced to a cerebellar screw and other brain regions were referenced to a frontal screw, demonstrating that observed gamma dynamics reflect synchronous oscillations rather than high frequency activity in the reference (Figure S7B). These changes were specific to the BLA-mPFC-vHPC circuit, as the dHPC (n=9) was not strongly engaged in gamma-gamma coupling with the BLA (figure 6A).

Given the strong, zero-phase lag synchrony of mPFC-BLA-vHPC fast gamma oscillations, we tested the possibility that safety modulated gamma in the mPFC and vHPC, like gamma in the BLA. Fast gamma power was lower during the CS+ than the CS− in the mPFC of discriminators (Figure 6B), with no change in the slow gamma or higher spectral ranges (p>.05; data not shown). As in the BLA, better behavioral discrimination between the CS+ and CS− correlated with higher mPFC fast gamma power in the CS− (r=.52; p<.01; Figure 6B). Consistent with these being safety-related changes, individual animals showed an inverse correlation between freezing rate on a given trial and fast gamma power in the mPFC, as in the BLA (Figure S7C). Interestingly, no significant safety-related changes in vHPC gamma were found (Figure 6B), despite strong gamma synchrony with the other two brain structures (Figure 6A).

We reasoned that these corresponding changes in mPFC and BLA gamma power might reflect periods of increased gamma-gamma synchrony. Indeed, the probability of mPFC-BLA near-zero phase lag synchrony (Supplementary Experimental Procedures) was significantly higher during the CS− in discriminators (sign-rank, p<.05; Figure 6C) but not generalizers (p>.05), and there was a corresponding linear correlation between the change in fast gamma synchrony and discrimination score across animals (Figure 6C; r=.45, p=.04). These findings indicate that the mPFC and BLA exhibit strong synchrony in the fast gamma range during periods of relative safety.

To further explore the dynamics of the mPFC-BLA-vHPC circuit, we used the Granger causality index (GCI) to model potential causal influences using phase and power

information. The GCI infers the strength of directional influences between LFPs by testing whether one LFP (e.g., from the mPFC) is useful in predicting the other (e.g., from the BLA), and vice versa. For fast gamma, we found significantly stronger Granger causality for the mPFC→BLA direction than the BLA→mPFC direction (Figure 7D; $p < .05$, sign-rank), suggesting that on average, fast gamma frequency activity in the mPFC tends to be predictive of future changes in the BLA. Granger causality similarly suggested predominant BLA→ vHPC and mPFC→vHPC directionality ($p < 0.05$, sign-rank), suggesting that gamma activity flows from the mPFC to the BLA and then to the vHPC (Figure 6F). Moreover, the mPFC->BLA Granger lead strength, which we defined for each animal as $GCI^{mPFC \rightarrow BLA} / (GCI^{mPFC \rightarrow BLA} + GCI^{BLA \rightarrow mPFC})$, was correlated with discrimination (Figure 6E, $r=.50$, $p<.05$), such that stronger evidence for an mPFC lead was present during the CS− compared to the CS+. These findings support a functional role for directionality in the gamma range during fear discrimination, and suggest that safety is associated with a shift towards greater mPFC-to-BLA directionality, similar to our previous findings with theta-frequency synchrony (Likhtik et al., 2014).

Dynamic switches in theta-gamma coupling

Given that gamma couples strongly to theta oscillations, we reasoned that the observed mPFC-to-BLA gamma directionality is at least partly a result of safety-related directional theta information transfer from the mPFC to BLA (Likhtik et al., 2014). We therefore examined the relationship between gamma and theta activity within and across structures in the BLA-mPFC-vHPC network. Theta-gamma coupling was qualitatively similar in all three brain regions, with slow and fast gamma coupling to similar phases of theta (Figure 6A; n=23, BLA; n=17, vHPC; n=27, mPFC). We also found considerable theta-gamma coupling across structures (Figure 7B), consistent with a highly interconnected network. Intriguingly, fast gamma oscillations in the BLA had significantly stronger coupling to mPFC theta oscillations than to local BLA theta oscillations ($p<.001$, Figure 7B). By contrast, mPFC gamma oscillations were better modulated by local mPFC theta than BLA theta ($p<.001$; data not shown). We were concerned that strong mPFC theta-BLA fast gamma coupling could arise if the gamma recorded in the BLA was not locally generated. To address this caveat, we re-examined phase-locking of BLA multi-unit recordings to BLA fast gamma as well as to gamma in the vHPC and mPFC. 76% of significantly phase-locked multi-units (40% of multi-unit recordings, Bonferonni-corrected, $p<.0125$, Figure 7B) were phase-locked to the BLA (59% to the BLA alone, and 17% to the BLA and at least one other brain structure). Only 24% (8% of the total) were significantly phase-locked to another structure but not the BLA. These data confirm that BLA units are most strongly phase-locked to local BLA gamma, as one would expect for a locally generated oscillation.

In Figure 3 we showed that local BLA theta-BLA gamma coupling increases with CS+ presentation, arguing that local theta-gamma coupling is associated with fear. Yet here we present evidence of even stronger coupling of BLA gamma to mPFC theta, which was previously implicated in safety signaling (Likhtik et al., 2014). These findings suggested that mPFC and BLA theta might compete for control of the BLA fast gamma-generating circuit. According to this idea, during fear, local BLA theta modulates BLA gamma, reducing fast gamma power, while during safety, mPFC theta inputs predominate, increasing fast gamma

power. To further test this hypothesis, we examined the relationship between BLA-mPFC theta directionality and gamma frequency changes in the BLA. To quantify directionality in the theta range, we calculated the cross-correlation between the theta power in the BLA and mPFC in short (1 s) time windows; the lag at the peak of this cross-correlation indicates predominant theta directionality (Supplementary Experimental Procedures; Adhikari et al., 2010a; Likhtik et al., 2014). We observed that on trials with a greater probability of mPFC theta lead, there was an increase in BLA fast gamma power, while increased probability of BLA lead was associated with a drop in fast gamma power (Figure 7D). This relationship held true overall for the population by multiple linear regression (mPFC lead: $p=5.2 \times 10^{-5}$; BLA lead: p=.0011, MLR; data not shown). On a moment-to-moment basis, windows in which the BLA led had lower fast gamma power than windows in which the mPFC led (Figure 7E; p<.05, sign-rank).

Along with shifts in theta frequency lead, theta-gamma coupling changed dynamically as well, such that BLA fast gamma was strongly coupled to local BLA theta in some epochs, and to mPFC theta in others. On trials when coupling to mPFC theta predominated, gamma power was higher; when coupling to BLA theta predominated, gamma power was lower (Figure 7F). These findings suggest a competitive mechanism between BLA and mPFC theta-frequency inputs for control of the fast gamma circuit within the BLA, and provide evidence for a relationship between mPFC control over BLA gamma and safety signals.

Theta-gamma dynamics and safety

Our data from fear conditioning were highly suggestive of an mPFC-to-BLA safety signal in the gamma range. To confirm that the same physiological correlates could be observed in other safe contexts, we first evaluated changes throughout extinction of conditioned fear, as animals learned that the previously aversive CS+ no longer posed a threat. After an additional two days of exposure to CSs without shock, animals returned to a baseline level of freezing (~20%; Figure 8A; n=11). Throughout extinction, there was a steady increase in BLA and mPFC fast gamma power during tone presentations (Figure 8B, C; p<.05, MLR). Notably, this effect was seen both for animals that began as discriminators and those that began as generalizers (data not shown), suggesting that these changes reflect safety signals, rather than the active process of discrimination, which could not be disentangled during fear recall. At the same time, we saw an enhancement of the $GCI^{mPFC \rightarrow BLA}$ (Figure 8D; $p=4.7 \times 10^{-5}$, MLR), without a corresponding change in the $GCI^{BLA \rightarrow mPFC}$ (p=.97), suggesting that the observed increase in fast gamma power was the result of enhanced mPFC input to the BLA. These data are consistent with recently reported changes in mPFC-BLA theta directionality during extinction (Lesting et al., 2013), and suggest that the enhancement of synchronous fast gamma oscillations of the mPFC-BLA circuit is a fundamental mechanism for suppression of fear responses during both fear discrimination and extinction.

Both fear discrimination and extinction probe fear and safety using learned stimuli, but a true safety signal should also apply to innate behavior. To probe safety in an innate anxiety paradigm, we evaluated data from the same animals prior to fear conditioning in a brightly lit open field. Most mice tend to avoid the center, staying near the walls of the periphery, while some mice actively explore the entire environment (Figure 8D). We evaluated changes

in fast gamma for both anxious (<10% center time, n=9) and non-anxious (>10% center time, n=6) animals (defined as in Likhtik et al., 2014). As expected, a safety-related increase in fast gamma power was observed only in anxious mice as they moved further from the anxiogenic center (Figure 8E; p=.003, MLR, zone vs. fast gamma power; non-anxious mice, p=.463). As during fear conditioning, we found enhanced mPFC Granger lead strength towards the periphery for anxious mice (Figure 8F; p=.026, MLR) but not non-anxious mice (p=.565). It is notable that anxious and non-anxious animals were equally likely to go on to be discriminators (56% and 66%, respectively), suggesting that these results reflect a continuously evaluated representation of safety, rather than persistent animal-to-animal circuit differences. Taken together, these data support BLA fast gamma coupling to mPFC input as a safety signal in both learned and innate fear paradigms.

Discussion

Fear states involve amygdala interactions with an extended network and in particular, its dense reciprocal connectivity with the mPFC. In this study, we investigated oscillatory network dynamics during fear discrimination. Fear-conditioned tones elicited increased theta-fast gamma coupling within the BLA, while the power of these fast gamma oscillations was paradoxically decreased. During the explicitly unpaired CS−, which signaled relative safety, fast gamma power was increased compared to the CS+, despite weaker coupling to local BLA theta. This elevated gamma power was associated with a predominant mPFC-to-BLA directionality and increased entrainment of BLA gamma by mPFC theta. A similar increase in BLA gamma power and switch towards an mPFC-to-BLA directionality was also seen after extinction of learned fear, and in the safe areas within the open field, a test of innate anxiety. Thus the data support a common mechanism for the suppression of both learned and innate fear responses, involving directional information flow from the mPFC to the BLA and mPFC entrainment of fast gamma-resonant circuits in the BLA.

Based on these findings, along with results from a number of studies demonstrating enhanced theta-frequency synchrony during fear-related behavior (Lesting et al., 2011, Seidenbecher et. al., 2003, Popa et. al., 2010, Likhtik et al, 2014), we propose the following conceptual model (Figure S8). During fear, a threat-related theta signal strongly and reciprocally synchronizes BLA and mPFC, coordinating local gamma activity within each structure and leading to strong local theta/gamma coupling during the CS+. During safety, theta frequency inputs from the mPFC to the BLA predominate, suppressing the fear response via the BLA fast gamma circuit. The CS− is therefore characterized by strong, directional thetatheta synchrony from the mPFC to the BLA (Likhtik et al., 2014) and strong modulation of BLA gamma by mPFC theta (reported here). Because mPFC theta activity drives gamma generators locally in the mPFC and distally in the BLA, the CS− is also associated with strong mPFC-BLA gamma synchrony. This long-range gamma synchrony is predominantly directional from the mPFC to the BLA, either because the mPFC theta drives mPFC gamma with a shorter delay than BLA gamma, or because of directional projections from gamma generating circuits in the mPFC to the BLA. This model is consistent with the broadly accepted role of the mPFC in suppressing amygdala-generated fear behaviors, and has several mechanistic and conceptual implications that deserve further discussion.

mPFC-BLA interactions during fear and safety

The roles of the mPFC and BLA in acquisition and extinction of conditioned fear responses are well-characterized. While the prevailing model is that amygdala output generates fear responses and input from the PFC inhibits fear behavior (Maren and Quirk, 2004; Pape and Pare, 2010), this description is oversimplified. For example, silencing or disrupting plasticity in either structure impairs both acquisition and extinction of learned fear (Sierra-Mercado et al., 2011), suggesting that both the mPFC and BLA have roles to play in fear expression and suppression. Furthermore, a number of experiments have suggested that specific subregions within the mPFC might play opposing roles in the regulation of fear, with output from the prelimbic (PL) area facilitating fear and output from the infralimbic (IL) suppressing fear (Knapska et al., 2012; Sierra-Mercado et al., 2011; Vidal-Gonzalez et al., 2006). The dynamic interactions described here further add to this complexity; fear and safety can be seen as different modes of BLA-mPFC communication.

More precise experimental techniques are beginning to define the microcircuit components within the BLA-mPFC circuit responsible for the expression and regulation of fear. Fear learning recruits specific populations of neurons within the amygdala, which are required for fear recall (Han et al., 2009). Different subpopulations of amygdala neurons are recruited during fear memory recall and after extinction (Herry et al., 2008), with fear recall neurons preferentially projecting to the PL and extinction neurons preferentially projecting to the IL (Senn et al., 2014). Thus, the observed involvement of the PL in fear (Burgos-Robles et al., 2009) and the IL in safety (Milad and Quirk, 2002) may be defined by segregated amygdala afferents.

While mPFC LFP recordings cannot distinguish between PL- and IL-derived activity, the dynamic changes in network synchrony reported here underscore the complex role that the mPFC plays in learning about danger and safety. Work in primates has shown that the dorsal anterior cingulate (dACC), the primate homologue of the rodent PL, adjusts amygdala firing when stimuli switch valence during aversive-reinforcement learning (Klavir et al., 2013). Given the findings presented here, such dACC-toamygdala directionality could account for the safety signal-evoked firing acquired in the primate amygdala during training (Genud-Gabal et al., 2013). Human data accentuate the flexibility of this circuit during learning. Consistent with data from animal models, the dorsal ACC/mPFC are engaged during fear expression and early extinction, while the ventral ACC/mPFC (IL homologue) are active during late extinction (Etkin et al., 2011). On the other hand, safety engages both the dorsolateral PFC (Pollak et al., 2010) and ventromedial PFC (Schiller et al., 2008). Thus, the role of different PFC and ACC subdivisions in safety signaling remains to be elucidated.

It is unclear which circuit level changes mediate these shifts in network dynamics, though recent work has provided data on how communication from the mPFC to the BLA is altered after extinction training. Cho et al. (2013) showed that extinction altered feed-forward excitatory-inhibitory balance for mPFC inputs to the BLA reducing mPFC-evoked EPSPs in pyramidal cells but preserving excitatory drive onto BLA interneurons. Thus, the mPFC recruits local circuit interneurons, including intercalated cells (Amano et al., 2010), to mediate fear reduction during extinction (Likhtik et al., 2008). This is consistent with data from safety learning, where a safety-associated CS evoked a decreased lateral amygdala LFP

response while a fear-associated CS evoked an enhanced LFP response (Rogan et al., 2005). These findings are consistent with the proposed model which suggests that a fast gamma-generating neuronal circuit, modulated by mPFC input, is engaged during relative safety, suppressing fear. The finding that extinction induces remodeling of perisomatic inhibitory synapses from parvalbumin positive (PV+) interneurons onto pyramidal cells in the amygdala (Trouche et al., 2013) raises the intriguing possibility that this interneuron subtype may participate in the putative gamma-generating microcircuit; PV+ interneurons are implicated in gamma generation in the hippocampus and neocortex (Lasztóczi and Klausberger, 2014; Sohal et al., 2009).

The activity of PV+ interneurons may also relate to the inverse relationship between gamma power and theta-gamma coupling that we observed. Courtin et al. (2014) demonstrated that the suppression of PV+ interneuron activity in the PL is necessary and sufficient for inducing tone-evoked theta synchrony within the mPFC and freezing. While Courtin et al. did not record from the BLA during inhibition of PV+ neurons in the PL, it is possible that inhibiting these PV+ interneurons also increased mPFC-BLA theta synchrony, enhancing fear responses. Conversely, the activation of mPFC PV+ interneurons may drive circuits required for the directional gamma synchrony and increasing gamma power we report during the CS−.

The role of the ventral hippocampus

The ventral hippocampus also constitutes an important node in the mPFC-BLA-vHPC anxiety-processing network and its role has recently come under increased investigation. Inactivation of vHPC interferes with expression of innate anxiety, fear recall and consolidation of extinction learning (Kjelstrup et al., 2002; Sierra-Mercado et al., 2011). Studies looking at interactions between the BLA, mPFC and vHPC have begun to reveal interesting parallels in the way that information flow between these three areas underlies fear and anxiety. For example, activating region-specific BLA inputs to the vHPC and mPFC increases expression of innate anxiety and learned fear, respectively (Sotres-Bayon et. al., 2012, Senn et. al., 2014, Felix-Ortiz et al., 2013). Conversely, vHPC inputs to both the BLA and mPFC may be important for providing contextual information about emotional content of learned and innate experience. In support of this idea, anxiety-coding mPFC neurons are phase locked to vHPC inputs (Adhikari et. al., 2011) and vHPC inputs to the mPFC are engaged in dampening contextual fear after extinction (Hugues and Garcia, 2007, Sotres-Bayon et. al., 2012). Similarly, vHPC inputs to the BLA become more active during contextual fear renewal (Knapska et al., 2012; Orsini et al., 2011). The differential involvement of the vHPC in mediating increases in innate anxiety and decreases in conditioned fear suggests that it gates innate and learned emotional processing via different mechanisms. Given the substantial body of literature about the importance of vHPC for both fear expression and extinction, we were surprised to find that though the vHPC showed synchrony with the mPFC and BLA in the theta and gamma range, its LFP did not show robust safety-related changes during fear discrimination. This may be because we probed auditory fear associations in a novel context, whereas most previous work assayed vHPC involvement in learned fear paradigms involving contextual conditioning.

Gamma oscillations and dynamic input switching

During the CS+, BLA gamma is strongly coupled to local theta, whereas during the CS−, it shifts to couple more strongly with theta from the mPFC. This dynamic switch suggests that in the amygdala, as in the better-studied HPC, theta-gamma coupling provides a framework for input selection. In the HPC, theta-nested gamma organizes the firing of neural ensembles on different phases of the ongoing theta oscillation (Lisman and Buzsáki, 2008; Lisman and Jensen, 2013). Distinct fast and slow bands of theta-coupled gamma oscillations (Belluscio et al., 2012) differentially synchronize the CA1 region with input from the entorhinal cortex and CA3, respectively (Colgin et al., 2009). Switches between these two processing modes permit neurons in CA1 to represent prospective and retrospective spatial locations, depending upon the dominant input (Bieri et al., 2014; Yamamoto et al., 2014). Here we find that the fast gamma band within the BLA is preferentially coupled to mPFC theta input, and that this input is strongest during periods of safety. Periods of threat, by contrast, are associated with increased coupling to locally recorded theta. It is unclear from our data whether slow gamma in the BLA has a different input preference or behavioral analog compared to fast gamma. Nonetheless, both the HPC and BLA appear to dynamically switch between different gamma frequency modes, mediating input selection.

Conclusion

Within the amygdala, the consequences of mode switching are presumably read out in the behavior of the animal. Fear discrimation between learned or innnate stimuli engages synchronous activity within the BLA-mPFC circuit. Safety involves a specific directionality to this synchrony, such that theta activity within the mPFC modulates a gamma-generating circuit in the BLA, presumably suppressing fear and anxiety-related behaviors. Future experiments aimed at exploring the microcircuitry underlying these phenomena and causally testing their relationship to behavior will further clarify the mechanisms by which the BLA-mPFC circuit distinguishes fear and safety.

Experimental Procedures

The current manuscript presents additional analyses of data overlapping with previously described experiments (Likhtik et al., 2014). A total of 21 male 129Sv/EvTac wild-type mice (3-6 months old, Taconic Farms, Germantown, NY) were used in Likhtik et al., 2014; 9 additional animals are included in the current manuscript. Sample sizes reported include only animals with verified, accurate placements in the relevant brain regions. All procedures were conducted in accordance with National Institutes of Health regulations and approved by the Columbia University and New York State Psychiatric Institute Institutional Animal Care and Use Committees.

Microdrive Construction

Microdrive were constructed and implanted as previously described (Likhtik et al., 2014). Briefly, craniotomies were made using AP and ML coordinates from bregma and DV coordinates from brain surface (provided in mm). Tungsten stereotrodes were implanted in the BLA (-2.06 AP, 3.15 ML, -3.4 DV) and tungsten wires were implanted in the mPFC (+1.65 AP, .3 ML, -1.6 DV), dorsal and ventral CA1 (-1.85 AP, 1.25 ML, -1.15 DV; -3.16

AP, 3.0 ML, -3.7 DV) under ketamine/xylazine anesthesia, supplemented with isoflurane. Skull screws over the cerebellum and frontal pole served as ground and reference, respectively.

Behavioral Protocol and Data Acquisition

After recovery to pre-surgical body weight, mice were food restricted to 85% body weight to increase exploration, habituated to handling and recording in a small, familiar environment, and then in an open field. Three days later, animals were exposed to differential fear conditioning as previously described (Likhtik et al., 2014). Briefly, mice received 5-6 trials each of 8 kHz or white noise tones, counterbalanced and pseudo-randomly presented daily for three days. Each stimulus consisted of 30 pips lasting 50 ms. delivered at 1Hz. One tone type was paired with shock (CS+; 0.4 mA, 1 sec), and the other was explicitly unpaired (CS −).

Assessment of freezing behavior and neurophysiological data acquisition were performed as previously described (Likhtik et al., 2014) and took place on the fourth day. Each animal received five CS+ and CS− presentations without shocks in a novel context. The discrimination score was calculated for each animal, and was the difference between percent time spent freezing in CS+ and CS−. Multi- and single-units were bandpass-filtered (600-6000 Hz) and recorded at 32 kHz. LFP signals from all areas were bandpass filtered (1-1000 Hz), acquired at 1894 Hz, and referenced against the frontal screw; some recordings were simultaneously referenced to the cerebellar screw.

A subset of animals (n=11) were subsequently extinguished by repeating the ten presentations of each stimulus over two additional days; recordings were obtained throughout.

Data Analysis

Data was imported into Matlab (Natick, MA) for analysis. A combination of custom-written scripts and scripts provided by K. Harris (University College London, UK) were used for the analyses. Multi-taper spectrograms were calculated with a time window of 256 samples, 1024 FFTs, and a time-bandwidth product (NW) of 1.5 (2 tapers). To calculate the power envelope and phase of ongoing theta and gamma oscillations, a bandpass filter was applied using a zero-phase-delay FIR filter with Hamming window (filter0, provided by K. Harris and G. Buzsáki, New York University, USA) and the Hilbert transform of the bandpass-filtered signal. Single units were clustered using Klustakwik (by Ken Harris, http://klustakwik.sourceforge.net/), using the first three principal components. Clusters were kept for analysis if signal-to-noise ratio ≥ 3 and their isolation distance was ≥ 10 using an 8-dimensional feature space. Additional details with regard to data analysis can be found in the Supplementary Experimental Procedures.

Statistics

Wilcoxon's sign-rank test was used for paired comparisons. Wilcoxon's rank-sum test was used for unpaired, independent observations. McNemar's test was used for proportions comparing two conditions (2 × 2 contingency tables). For circular statistics, the Rayleigh

test for unimodality was used throughout. For continuous analyses, Pearson's r was calculated. For correlations with multiple data points per animal, multiple linear regression (MLR) was performed in Matlab (regstats function). P-values indicate the significance of the explanatory variable of interest after accounting for within animal dependence. If given, r values refer to the full model. Error is reported as mean ± standard error of the mean (±SEM), unless otherwise noted.

Supplementary Material

Refer to Web version on PubMed Central for supplementary material.

Acknowledgments

We would like to thank A. Sirota of the University of Tubingen, Germany for helpful advice on analytic methods. This work was supported by grants from the NIMH to J.A.G (R01 MH081968 and P50 MH096891) and E.L. (F32 MH088103), by the Hope for Depression Research Foundation and the International Mental Health Research Organization (J.A.G.), and by the Charles H. Revson Foundation (E.L.). J.M.S. is supported through the Columbia University Medical Scientist Training Program.

References

Adhikari A, Sigurdsson T, Topiwala MA, Gordon JA. Cross-correlation of instantaneous amplitudes of field potential oscillations: A straightforward method to estimate the directionality and lag between brain areas. J Neurosci Meth. 2010a; 191:191–200.

Adhikari A, Topiwala MA, Gordon JA. Synchronized activity between the ventral hippocampus and the medial prefrontal cortex during anxiety. Neuron. 2010b; 65:257–269. [PubMed: 20152131]

Adhikari A, Topiwala MA, Gordon JA. Single units in the medial prefrontal cortex with anxiety-related firing patterns are preferentially influenced by ventral hippocampal activity. Neuron. 2011; 71:898–910. [PubMed: 21903082]

Amano T, Unal CT, Pare D. Synaptic correlates of fear extinction in the amygdala. Nat Neurosci. 2010; 13:489–U112. [PubMed: 20208529]

Bauer EP, Paz R, Pare D. Gamma oscillations coordinate amygdalo-rhinal interactions during learning. The Journal of neuroscience : the official journal of the Society for Neuroscience. 2007; 27:9369–9379. [PubMed: 17728450]

Belluscio MA, Mizuseki K, Schmidt R, Kempter R, Buzsáki G. Cross-Frequency Phase-Phase Coupling between Theta and Gamma Oscillations in the Hippocampus. J Neurosci. 2012; 32:423–435. [PubMed: 22238079]

Bieri KW, Bobbitt KN, Colgin LL. Slow and fast gamma rhythms coordinate different spatial coding modes in hippocampal place cells. Neuron. 2014; 82:670–681. [PubMed: 24746420]

Burgos-Robles A, Vidal-Gonzalez I, Quirk GJ. Sustained Conditioned Responses in Prelimbic Prefrontal Neurons Are Correlated with Fear Expression and Extinction Failure. J Neurosci. 2009; 29:8474–8482. [PubMed: 19571138]

Buzsáki G, Wang XJ. Mechanisms of Gamma Oscillations. Annu Rev Neurosci. 2012; 35:203–225. [PubMed: 22443509]

Cho JH, Deisseroth K, Bolshakov VY. Synaptic Encoding of Fear Extinction in mPFC-amygdala Circuits. Neuron. 2013; 80:1491–1507. [PubMed: 24290204]

Cho RY, Konecky RO, Carter CS. Impairments in frontal cortical gamma synchrony and cognitive control in schizophrenia. Proceedings of the National Academy of Sciences of the United States of America. 2006; 103:19878–19883. [PubMed: 17170134]

Colgin LL, Denninger T, Fyhn M, Hafting T, Bonnevie T, Jensen O, Moser MB, Moser EI. Frequency of gamma oscillations routes flow of information in the hippocampus. Nature. 2009; 462:353–U119. [PubMed: 19924214]

Courtin J, Chaudun F, Rozeske RR, Karalis N, Gonzalez-Campo C, Wurtz H, Abdi A, Baufreton J, Bienvenu TC, Herry C. Prefrontal parvalbumin interneurons shape neuronal activity to drive fear expression. Nature. 2014; 505:92–96. [PubMed: 24256726]

Courtin J, Karalis N, Gonzalez-Campo C, Wurtz H, Herry C. Persistence of amygdala gamma oscillations during extinction learning predicts spontaneous fear recovery. Neurobiol Learn Mem. 2013

Etkin A, Egner T, Kalisch R. Emotional processing in anterior cingulate and medial prefrontal cortex. Emotional processing in anterior cingulate and medial prefrontal cortex. Trends Cogn Sci. 2012; 15:85–93. [PubMed: 21167765]

Felix-Ortiz AC, Beyeler A, Seo C, Leppla CA, Wildes CP, Tye KM. BLA to vHPC inputs modulate anxiety-related behaviors. Neuron. 2013; 79:658–664. [PubMed: 23972595]

Fries P. Neuronal gamma-band synchronization as a fundamental process in cortical computation. Annu Rev Neuroscience. 2009; 32:209–224.

Genud-Gabai R, Klavir O, Paz R. Safety signals in the primate amygdala. J Neurosci. 2013; 33:17986–17994. [PubMed: 24227710]

Han J-H, Kushner SA, Yiu AP, Hsiang H-L, Buch T, Waisman A, Bontempi B, Neve RL, Frankland PW, Josselyn SA. Selective Erasure of a Fear Memory. Science. 2009; 323:1492–1496. [PubMed: 19286560]

Headley DB, Weinberger NM. Fear Conditioning Enhances Gamma Oscillations and Their Entrainment of Neurons Representing the Conditioned Stimulus. J Neurosci. 2013; 33:5705–+. [PubMed: 23536084]

Herry C, Ciocchi S, Senn V, Demmou L, Muller C, Luthi A. Switching on and off fear by distinct neuronal circuits. Nature. 2008; 454:600–U628. [PubMed: 18615015]

Hugues S, Garcia R. Reorganization of learning-associated prefrontal synaptic plasticity between the recall of recent and remote fear extinction memory. Learning & memory (Cold Spring Harbor, NY). 2007; 14:520–524.

Kjelstrup KG, Tuvnes FA, Steffenach HA, Murison R, Moser EI, Moser MB. Reduced fear expression after lesions of the ventral hippocampus. Proc Natl Acad Sci U S A. 2002; 99:10825–10830. [PubMed: 12149439]

Klavir O, Genud-Gabai R, Paz R. Functional connectivity between amygdala and cingulate cortex for adaptive aversive learning. Neuron. 2013; 80:1290–1300. [PubMed: 24314732]

Knapska E, Macias M, Mikosz M, Nowak A, Owczarek D, Wawrzyniak M, Pieprzyk M, Cymerman IA, Werka T, Sheng M, et al. Functional anatomy of neural circuits regulating fear and extinction. Proceedings of the National Academy of Sciences. 2012

Lasztóczi B, Klausberger T. Layer-Specific GABAergic Control of Distinct Gamma Oscillations in the CA1 Hippocampus. Neuron. 2014; 81:1126–1139. [PubMed: 24607232]

Lesting J, Daldrup T, Narayanan V, Himpe C, Seidenbecher T, Pape HC. Directional theta coherence in prefrontal cortical to amygdalo-hippocampal pathways signals fear extinction. PloS one. 2013; 8:e77707. [PubMed: 24204927]

Lesting J, Narayanan RT, Kluge C, Sangha S, Seidenbecher T, Pape HC. Patterns of coupled theta activity in amygdala-hippocampal-prefrontal cortical circuits during fear extinction. PloS one. 2011; 6:e21714. [PubMed: 21738775]

Likhtik E, Popa D, Apergis-Schoute J, Fidacaro GA, Pare D. Amygdala intercalated neurons are required for expression of fear extinction. Nature. 2008; 454:642–645. [PubMed: 18615014]

Likhtik E, Stujenske JM, Topiwala MA, Harris AZ, Gordon JA. Prefrontal entrainment of amygdala activity signals safety in learned fear and innate anxiety. Nat Neurosci. 2014; 17:106–113. [PubMed: 24241397]

Lisman J, Buzsáki G. A neural coding scheme formed by the combined function of gamma and theta oscillations. Schizophrenia Bull. 2008; 34:974–980.

Lisman JE, Jensen O. The theta-gamma neural code. Neuron. 2013; 77:1002–1016. [PubMed: 23522038]

Maren S, Quirk GJ. Neuronal signalling of fear memory. Nat Rev Neurosci. 2004; 5:844–852. [PubMed: 15496862]

Milad MR, Quirk GJ. Neurons in medial prefrontal cortex signal memory for fear extinction. Nature. 2002; 420:70–74. [PubMed: 12422216]

Orsini CA, Kim JH, Knapska E, Maren S. Hippocampal and prefrontal projections to the basal amygdala mediate contextual regulation of fear after extinction. J Neurosci. 2011; 31:17269–17277. [PubMed: 22114293]

Pape HC, Narayanan RT, Smid J, Stork O, Seidenbecher T. Theta activity in neurons and networks of the amygdala related to long-term fear memory. Hippocampus. 2005; 15:874–880. [PubMed: 16158424]

Pape HC, Pare D. Plastic Synaptic Networks of the Amygdala for the Acquisition, Expression, and Extinction of Conditioned Fear. Physiological Reviews. 2010; 90:419–463. [PubMed: 20393190]

Pape HC, Pare D, Driesang RB. Two types of intrinsic oscillations in neurons of the lateral and basolateral nuclei of the amygdala. J Neurophysiol. 1998; 79:205–216. [PubMed: 9425192]

Paz R, Bauer EP, Pare D. Theta synchronizes the activity of medial prefrontal neurons during learning. Learning & Memory. 2008; 15:524–531. [PubMed: 18612069]

Pollak DD, Rogan MT, Egner T, Perez DL, Yanagihara TK, Hirsch J. A translational bridge between mouse and human models of learned safety. Annals of Medicine. 2010; 42:127–134.

Popa D, Duvarci S, Popescu AT, Lena C, Pare D. Coherent amygdalocortical theta promotes fear memory consolidation during paradoxical sleep. P Natl Acad Sci USA. 2010; 107:6516–6519.

Popescu AT, Popa D, Pare D. Coherent gamma oscillations couple the amygdala and striatum during learning. Nat Neurosci. 2009; 12:801–807. [PubMed: 19430471]

Ray S, Maunsell JH. Different origins of gamma rhythm and high-gamma activity in macaque visual cortex. PLoS biology. 2011; 9:e1000610. [PubMed: 21532743]

Rogan MT, Leon KS, Perez DL, Kandel ER. Distinct neural signatures for safety and danger in the amygdala and striatum of the mouse. Neuron. 2005; 46:309–320. [PubMed: 15848808]

Schiller D, Levy I, Niv Y, LeDoux JE, Phelps EA. From Fear to Safety and Back: Reversal of Fear in the Human Brain. J Neurosci. 2008; 28:11517–11525. [PubMed: 18987188]

Seidenbecher T, Laxmi TR, Stork O, Pape HC. Amygdalar and Hippocampal Theta Rhythm Synchronization During Fear Memory Retrieval. Science. 2003; 301:846–850. [PubMed: 12907806]

Senn V, Wolff SB, Herry C, Grenier F, Ehrlich I, Grundemann J, Fadok JP, Muller C, Letzkus JJ, Luthi A. Long-range connectivity defines behavioral specificity of amygdala neurons. Neuron. 2014; 81:428–437. [PubMed: 24462103]

Sierra-Mercado D, Padilla-Coreano N, Quirk GJ. Dissociable roles of prelimbic and infralimbic cortices, ventral hippocampus, and basolateral amygdala in the expression and extinction of conditioned fear. Neuropsychopharmacology : official publication of the American College of Neuropsychopharmacology. 2011; 36:529–538. [PubMed: 20962768]

Sohal VS, Zhang F, Yizhar O, Deisseroth K. Parvalbumin neurons and gamma rhythms enhance cortical circuit performance. Nature. 2009; 459:698–702. [PubMed: 19396159]

Sotres-Bayon F, Sierra-Mercado D, Pardilla-Delgado E, Quirk GJ. Gating of fear in prelimbic cortex by hippocampal and amygdala inputs. Neuron. 2012; 76:804–812. [PubMed: 23177964]

Tort AB, Komorowski RW, Manns JR, Kopell NJ, Eichenbaum H. Theta-gamma coupling increases during the learning of item-context associations. Proc. Natl. Acad. Sci. USA. 2009; 106:20942–20947. [PubMed: 19934062]

Trouche S, Sasaki JM, Tu T, Reijmers LG. Fear extinction causes target-specific remodeling of perisomatic inhibitory synapses. Neuron. 2013; 80:1054–1065. [PubMed: 24183705]

Vidal-Gonzalez I, Vidal-Gonzalez B, Rauch SL, Quirk GJ. Microstimulation reveals opposing influences of prelimbic and infralimbic cortex on the expression of conditioned fear. Learning & Memory. 2006; 13:728–733. [PubMed: 17142302]

Yamamoto J, Suh J, Takeuchi D, Tonegawa S. Successful execution of working memory linked to synchronized high-frequency gamma oscillations. Cell. 2014; 157:845–857. [PubMed: 24768692]

Highlights

- Two bands of theta-nested gamma in the BLA during fear expression
- BLA cells that phase-lock to fast gamma increase firing during safety
- Fast gamma coupled to BLA theta during fear, to mPFC theta during safety
- mPFC-to-BLA fast gamma directionality during safety in three behavioral paradigms

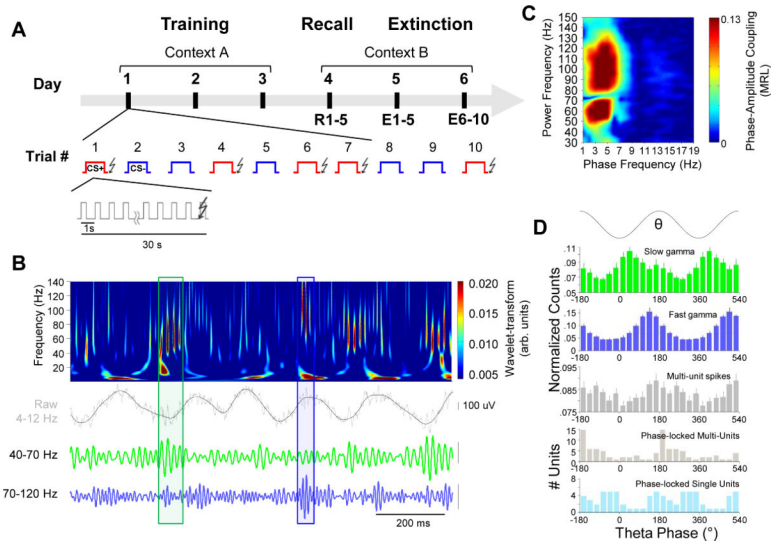

Figure 1. Two types of BLA gamma frequency oscillations are coupled to theta during fear recall

(A) Experimental protocol. See text for detailed description.

(B) Wavelet transform (color plot) of BLA LFP (gray) recorded during recall session (Day 4). Lower traces, slow (40-70 Hz, green) and fast (70-120 Hz, blue) gamma events, occurring at distinct phases of the theta oscillation (black). Boxes indicate representative high-amplitude gamma events in each frequency band.

(C) Phase-Amplitude comodugram of a representative BLA LFP recording demonstrating modulation of high frequency power (y-axis) by low frequency oscillation phase (x-axis). Warm colors indicate stronger modulation; note the prominent modulation of separate slow (40-70 Hz) and fast (70-120 Hz) gamma peaks.

(D) Histograms for the occurrence of slow gamma troughs, fast gamma troughs and multi-unit spikes (top three panels) and the preferred phase of significantly phase-locked ($p < .05$, Rayleigh test) multi-units (n=48) and single units (n=38; bottom two panels) relative to phases of the theta (4-12 Hz) oscillation. Error bars, here and throughout, are +/− SEM, except as otherwise noted.

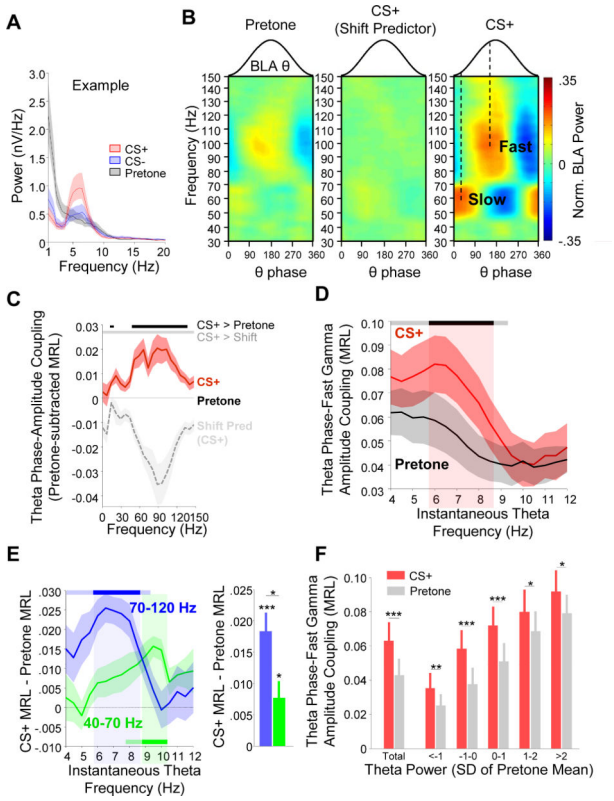

Figure 2. BLA theta-gamma coupling increases during conditioned fear

(A) Example power spectrum of BLA LFP during pretone (black), an aversive CS+ (red), and a neutral CS− (blue). Presentation of an aversive CS+ elicits higher BLA theta power (peak at 6Hz).

(B) Example comodugrams of theta–gamma coupling during pretone (left; 30s before tone), CS+ (right; during tone), and shift predictor of CS+ data (middle).

(C) Mean theta-fast gamma coupling strength for CS+ (red) and shift predictor (gray) normalized to pre-tone (black line at 0, n=15). Significance lines (top): CS+/pretone (black) and CS+/shift predictor (gray) differences ($p < 0.05/21$, Bonferroni-corrected, sign-rank).

(D) Mean theta-fast gamma coupling strength as a function of instantaneous theta frequency (n=15). Significance lines (top): Gray (uncorrected, $p < 0.05$) and black (Bonferroni-corrected sign rank, $p < 0.05/15$).

(E) Change in theta-gamma coupling strength from pretone to CS+ for fast gamma (blue) and slow gamma (green) as a function of instantaneous theta frequency (left) and averaged across the theta range (right). Significance lines (top): Differences from pre-tone for each gamma frequency band. Light blue (uncorrected) and dark blue (Bonferroni-corrected, sign-rank, $p<0.5/15$).

(F) Theta phase-fast gamma amplitude coupling strength as a function of theta power, binned in multiples of SD from the mean of the pretone theta power. * $p < .05$, ** $p < .01$, *** $p < .001$, sign-rank.

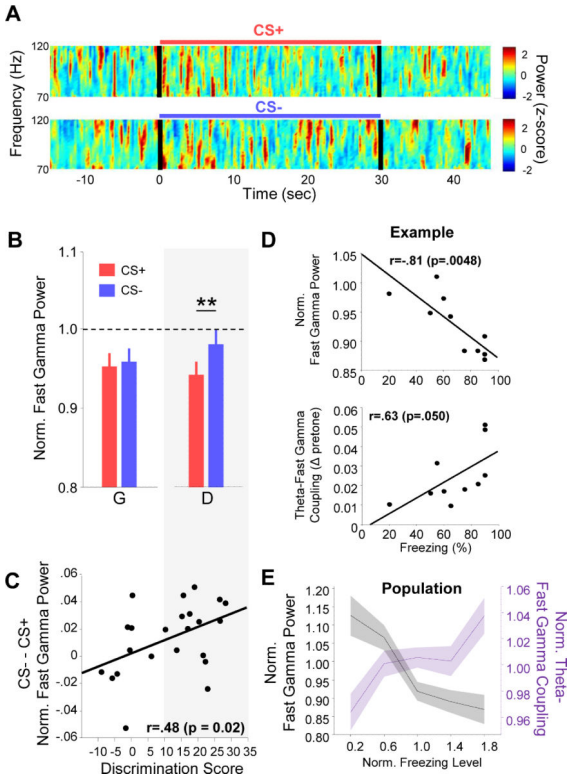

Figure 3. BLA fast gamma power decreases during conditioned fear

(A) Example multi-taper spectrograms of BLA LFP during a CS+ (top) and CS− (bottom) presentation. Power was normalized by z-scoring in each frequency range. Black lines, stimulus onset and offset.

(B) Fast gamma power during CS+ (red) and CS− (blue) presentations for Discriminators (D) and Generalizers (G). ** p <.01, sign-rank.

(C) The difference between CS− and CS+ fast gamma power plotted by animal, as a function of discrimination score (CS+ - CS− percent freezing), with Pearson's r and p-value indicated. Grey box spanning panels (B) and (C) indicates data from the discriminator group.

(D) Fast gamma power (top) and theta-fast gamma coupling strength (bottom) as a function of freezing on a trial-by-trial basis for an example animal. Each symbol represents data from a single trial. Data are normalized to pretone values.

(E) Population data showing fast gamma power (black) and theta-fast gamma coupling (purple) as a function of freezing level ($p<.001$ and $p<.05$, respectively, MLR). All data is mean-normalized.

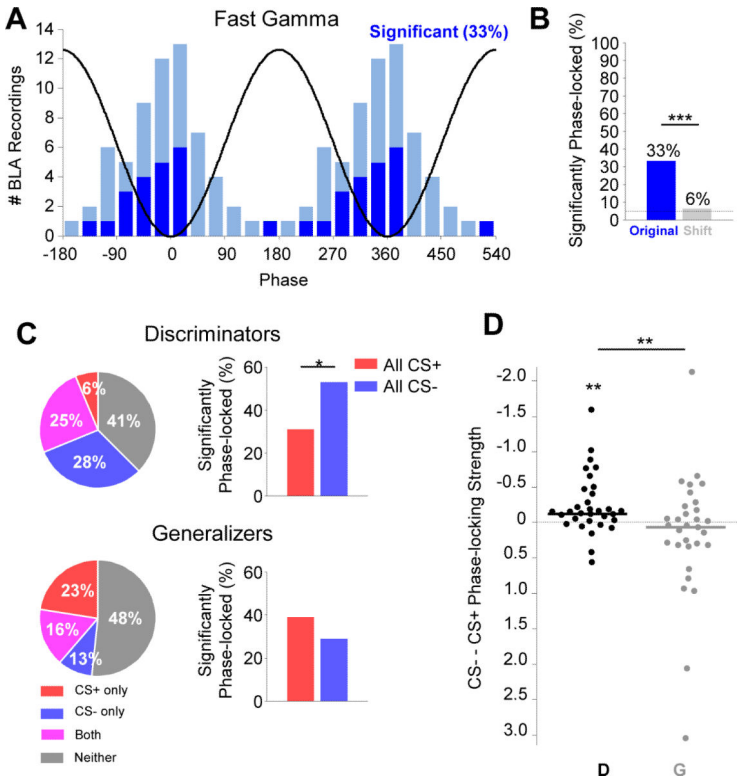

Figure 4. Increased fast gamma power during the CS− reflects synchronous neural firing

(A) Left, histogram of the preferred fast gamma phases for significantly (dark blue) and non-significantly (light blue) phase-locked multi-unit recordings ($p < .05$, Rayleigh test). Black line is a cartoon depiction of fast gamma oscillation phases.

(B) Percentage of multi-units significantly phase-locked to the fast gamma oscillation, compared to shift predictor. *** $p < .001$, McNemar's test.

(C) Left, pie charts illustrating the percentage of recordings demonstrating significant phase-locking to fast gamma during the CS+ only (red), CS− only (blue), or both (magenta) in Discriminators (top) and Generalizers (bottom). Right, percentage of significantly phase-locked units to CS+ and CS−, including overlap. * $p < .05$, McNemar's test.

(D) Change in multi-unit phase-locking strength to fast gamma from CS+ to CS− for discriminators (black, D) and for generalizers (grey, G). Mean change in discriminators is significantly different from 0 (** $p < .01$, sign-rank) and greater than in generalizers (** $p < .01$, rank-sum).

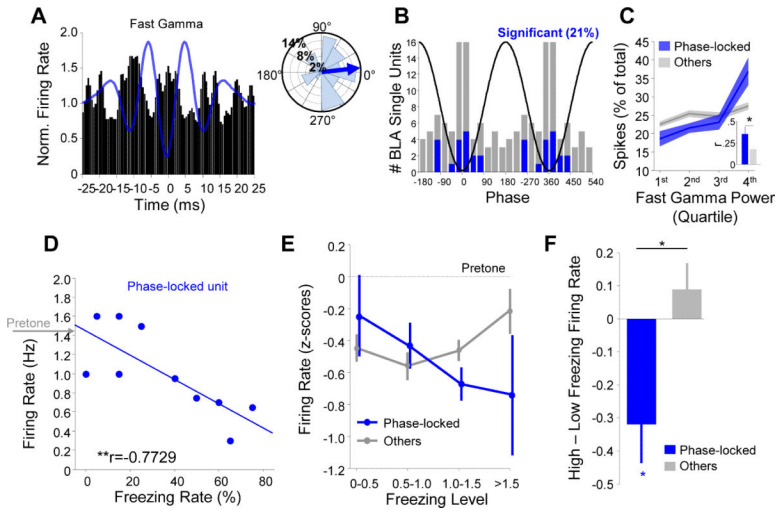

Figure 5. A subset of BLA single units synchronize with BLA fast gamma

(A) Left, fast gamma trough-triggered firing rate of an example single unit. Blue line, trough-triggered LFP. Right, distribution of spikes by gamma phase for this unit. Blue arrow indicates preferred phase.

(B) Histogram of the preferred fast gamma phases for significantly (blue) and non-significantly (gray) phase-locked single units ($p < .05$, Rayleigh test for both distributions). Oscillatory cycle is repeated for clarity.

(C) Spike distribution as a function of fast gamma power for significantly phase-locked cells (blue) and all other cells (gray). Fast gamma power was positively correlated with spike rate of both phase-locked ($r=0.5510$, $p=4.5 \times 10^{-6}$, MLR) and other cells ($r=0.2048$, $p=0.0011$, MLR), but this relationship was significantly stronger for phase-locked units (inset: phase-locked, r=0.35+/−.09; others, r=0.18+/−.04; p=.0232, rank-sum).

(D) Trial-by-trial firing rate as a function of freezing rate for an example fast gamma phase-locked unit (r=-.7729, ** $p < .01$). Gray arrow indicates mean pretone firing rate.

(E) Pretone-normalized firing rate as a function of mean-normalized freezing level averaged across all phase-locked (blue) and other (gray) single units. A significant effect of freezing was seen only on phase-locked cells ($p < .001$, MLR).

(F) Change in firing rate from low- to high-freezing trials for phase-locked (blue) and other (gray) single units. Decrease in rate for phase-locked units was significantly different from both 0 ($p < .05$, one-sample t-test) and from that in other units ($p < .05$, unpaired t-test).

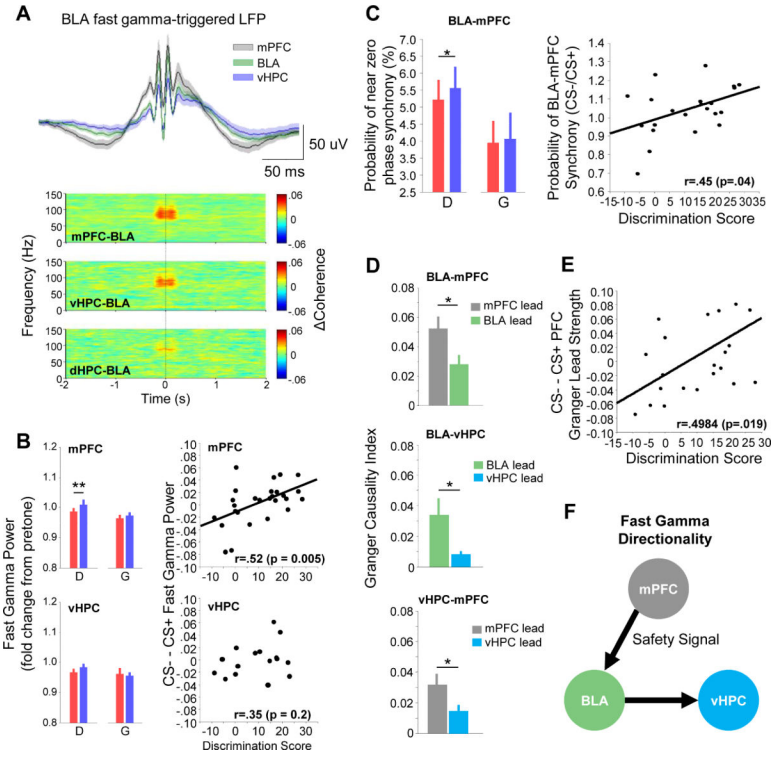

Figure 6. Synchrony and directionality of fast gamma in mPFC-BLA-vHPC circuit

(A) Top, BLA fast gamma trough-triggered LFPs from mPFC (black), BLA (green) and vHPC (purple). Bottom, fast-gamma trough-triggered spectral coherence for specific region pairs.

(B) Left, fast gamma power in the mPFC (top) and vHPC (bottom) during the CS+ (red) and CS− (blue) in discriminators (D) and generalizers (G). ** p < .01, sign-rank. Right, difference in fast gamma power between CS− and CS+ as a function of discrimination score for mPFC (top) and vHPC (bottom).

(C) Left, probability (over time) of observing near zero phase synchrony in the fast gamma range by CS type, for discriminators and generalizers. Right, ratio of probability by CS type, as a function of discrimination score. Each symbol represents data from an individual animal.

(D) Mean fast gamma Granger Causality Index for the mPFC-BLA (top), BLA-vHPC (middle), and vHPC-mPFC (bottom). Green, BLA lead; gray, mPFC lead; cyan, vHPC lead. *p<0.05, sign-rank.

(E) Difference in PFC to BLA Granger lead strength (see text) between CS− and CS+, as a function of discrimination score.

(F) Schematic of predominant directionality of fast gamma between mPFC, BLA, and vHPC, inferred from the data presented in D. A safety signal from the mPFC is propagated to the BLA, synchronizing fast gamma activity within the mPFC-BLA circuit.

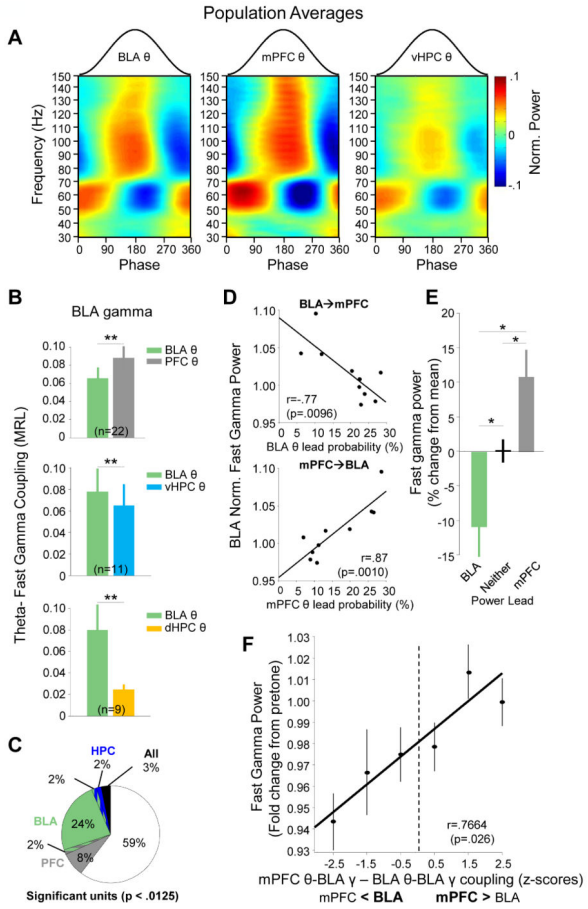

Figure 7. Increased BLA fast gamma is associated with mPFC-to-BLA theta directionality

(A) Mean CS+-evoked theta phase modulation of gamma frequency activity in the BLA (left, n=23), mPFC (middle, n=27), vHPC (right, n=17).

(B) CS+evoked phase-locking (MRL) of BLA fast gamma with its local theta oscillation (green) compared to BLA fast gamma phase locking with mPFC theta (grey, top panel), vHPC theta (cyan, middle panel), and dHPC theta (bottom panel). **p<.01, signrank.

(C) The number of BLA multi-unit recordings significantly phase-locked (p<.05/4, bonferroni corrected) to fast gamma oscillations in the mPFC (gray), BLA (green), vHPC (blue), mPFC and BLA (gray/green), BLA and vHPC (green/blue), and all structures (black). All recordings that phase-locked to the dHPC gamma oscillation (2%) also phase-locked to the vHPC gamma oscillation and were thus included with the vHPC in this depiction.

(D) Fast gamma power in the BLA, as a function of the percentage of time windows in which the BLA theta leads mPFC theta (top), or mPFC theta leads BLA theta (bottom). Data are from a representative animal; each symbol represents data from single trial.

(E) Population averages quantifying BLA fast gamma power for periods when instantaneous theta directionality corresponds to a BLA lead (green), no lead (black), or mPFC lead (gray).

(F) Gamma power as a function of the relative strength of coupling of BLA gamma to mPFC vs BLA theta (z-scored relative to BLA theta values).

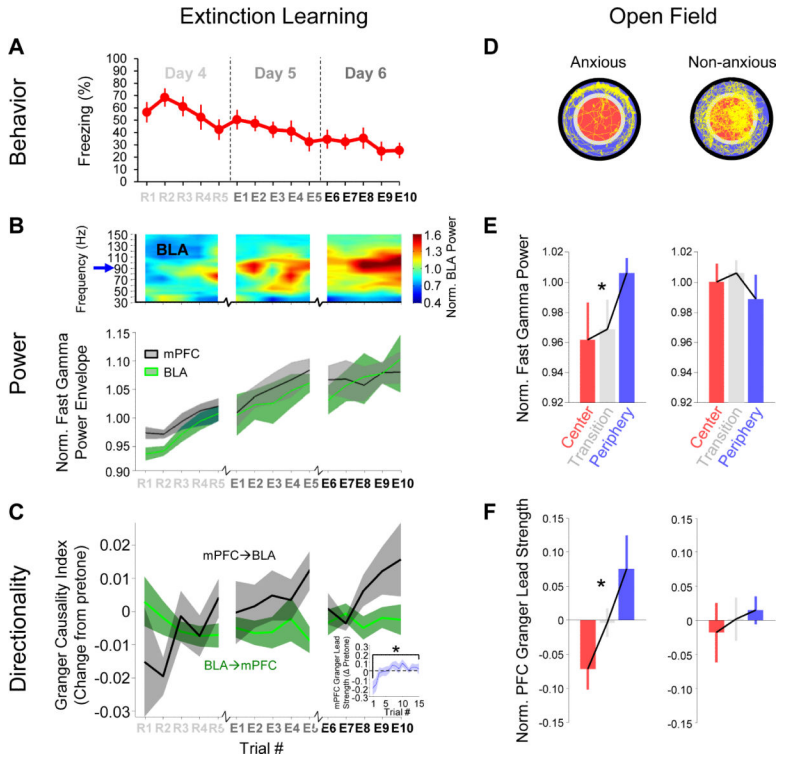

Figure 8. mPFC lead and BLA fast gamma power in extinction and the open field

(A) Freezing values for mice undergoing extinction during extinction training (CS+ data only).

(B) Top, power spectrogram of BLA LFP from a representative animal, showing trial to trial changes in fast gamma power through extinction. Bottom, population mean +/− SEM fast gamma amplitude through extinction for BLA (green) and mPFC (gray).

(C) Mean +/− Granger causality index, normalized by pretone value, for mPFC→BLA (gray) and BLA→mPFC (green) directions as a function of trial number. $GCI^{mPFC \rightarrow BLA}$ significantly increased throughout extinction ($p=4.7 \times 10^{-5}$, MLR), without a corresponding change in the $GCI^{BLA \rightarrow mPFC}$ ($p=.97$). Inset, relative mPFC granger lead strength (see text) from R1 to E10.

(D) Representative paths (yellow) of an anxious (left) and a non-anxious (right) mouse during exploration of a novel open field. Data from center (red), periphery (blue), and transition (gray) epochs was analyzed separately.

(E) Fast gamma power by open field zone for anxious (n=9, left) and non-anxious (n=6, right) mice.

(F) mPFC Granger lead strength by open field zone for anxious (left) and non-anxious (right) mice.